Array measurements of *S*-wave velocities from ambient vibrations

Fortunat Kind,* Donat Fäh and Domenico Giardini

Swiss Seismological Service, ETH Hönggerberg, CH-8093 Zürich, Switzerland

SUMMARY

The *S*-wave velocity is a very important factor in local hazard assessment. Direct measurement with conventional methods is very costly and therefore inexpensive and efficient methods are needed to make local hazard assessment more feasible. Techniques based on the analysis of recordings of ambient vibrations from small-scale arrays of sensors have become popular recently. One technique that is favoured by several research groups is the extraction of the dispersion curve by estimation of the *f*–**k** spectrum and its inversion for the *S*-wave velocity structure. This paper presents the results from an application based on high-resolution beamforming applied to the vertical component of the measurements. Synthetic ambient vibrations generated with a 2-D finite-difference code are used to illustrate and test the application. By superposition of random signals it is shown that the dispersion curve can be extracted even if 60 per cent of the wavefield consists of spatially uncorrelated signals. The errors in the phase velocities amount to less than 10 per cent. The dispersion curve can be extracted from the fundamental frequency of resonance upwards. Data from two real measurements are presented—from one site close to a city and another site within an industrial complex. The inverted *S*-wave velocity structures agree with reference data for the sites. The rule of thumb for the resolution of the method is confirmed.

Key words: array, earthquakes, Rayleigh waves, seismic ambient noise, seismic velocities, spectral analysis.

1 INTRODUCTION

For the estimation of the local site response in an earthquake the shear wave velocity is an important parameter on which ground motion amplification and soil liquefaction predictions are mainly based. However, there is a lack of reliable economic methods for determining this velocity. For *S*-wave reflection seismics it is difficult to generate sufficient energy to penetrate to larger depths and in the analysis of data the discrimination of *P*-wave and *S*-wave information is quite complex. Vertical seismic profiling or similar borehole seismics are better established, but they are very expensive to apply. An additional drawback of seismic methods is the high frequency range of the generated and measured waves, which is much higher then the range of interest in determination of site effects. An alternative to expensive seismic techniques is the derivation of *S*-wave velocities from ambient vibrations measured on an array of seismometers.

Ambient vibrations are composed mainly of surface waves, often dominated on the vertical component by the fundamental-mode Rayleigh wave. But the composition of the wavefield is quite complex as multiple wavelets are coming from all directions at the same

time. By extracting the dispersion of the surface waves and inverting it for the *S*-wave velocity structure, just exactly those data needed for the determination of local site effects at the frequencies of interest can be derived. The analysis of microtremor data for surface wave dispersion is an idea that has occupied seismologists for a long time. For example, Ramirez (1940) made experiments with a tripartite array and Toksöz (1964) also experimented with this concept. The critical point is the extraction of the surface wave dispersion, while for the inversion one of the many established methods can be used. We apply the *f*–**k**-spectrum estimation technique developed by Capon (1969) during the 1960s at the LASA wide aperture array. In the studies of Asten & Henstridge (1984), Horike (1985) and Matsushima & Okada (1990) the technique was applied successfully to ambient vibrations, and *S*-wave velocity structures could be derived. Succeeding works like that of Milana *et al.* (1996), Kawase *et al.* (1998), Liu *et al.* (2000) or Satoh *et al.* (2001a,b) also reported good results. Tokimatsu *et al.* (1992) used the method to resolve close surface *S*-wave structures with a resolution in the order of 1 m. A comprehensive review comparing methods with active and passive sources is given in Tokimatsu (1997). More research has been done by several Japanese authors on the subject cited in this review, but their results are published in Japanese only and are therefore inaccessible to us. The advantages of the technique are that it is not invasive and uses passive sources and is thus very inexpensive, that it penetrates to depths well below the usual 20–30 m of boreholes

*Now at: Converium Ltd, General Guisan Quai 26, 8022 Zürich, Switzerland.

and that it is applicable at sites where the level of ambient vibration prohibit seismic techniques. Therefore further development of the method to allow routine application would be very desirable.

After a brief introduction to the method we show a synthetic test to validate the technique, to illustrate the processing procedure and to demonstrate the applicability of the chosen approach. Then we show the results from two experimental measurements, done at sites in Switzerland where *S*-wave velocity information is available, to show how the relevant *S*-wave velocity information for determination of local site effects can be derived in a simple and cost-effective way.

2 MEASUREMENT METHOD

The method applied in this study for the data analysis is high-resolution beamforming (HRBF) developed by Capon (1969). This method uses the cross-power spectral densities of an array of sensors to estimate the f–$\mathbf{k}$ spectrum, refining it with coherency estimates. The estimation $\hat{P}(f, \mathbf{k})$ of the true f–$\mathbf{k}$ spectrum $P(f, \mathbf{k})$ is calculated as

$$\hat{P}(f, \mathbf{k}) = \left[\sum_{j=1}^{p} \sum_{l=1}^{p} q_{jl}(f) \exp[i\mathbf{k} \cdot (\mathbf{r}_j - \mathbf{r}_l)] \right]^{-1} \quad (1)$$

where $q_{jl}(f)$ are the elements of the inverse of the complex coherency matrix $f_{jl}(f)$ for sensors j and l ($[q_{jl}] = [f_{jl}]^{-1}$). The coherency matrix is calculated by the direct segment method, as described in Lacoss *et al.* (1969) and (Capon 1969):

$$f_{jl} = \frac{\sum_{n=1}^{M} S_{jn}(f)S_{ln}(f)}{\sqrt{\left(\sum_{n=1}^{M} S_{jn}^2 \right) \left(\sum_{n=1}^{M} S_{ln}^2 \right)}} \quad (2)$$

where M denotes the number of time segments used for the Fourier transform and S_{jn} denotes the value of the spectrum for frequency f. To avoid underflow problems in the calculation of the Fourier spectrum, the spectral values for frequency f, some smoothing was applied:

$$S_{jn}(f) = [S_{jn}(0.99f) + S_{jn}(f) + S_{jn}(1.01f)]/3. \quad (3)$$

The spectral values $S_{jn}(f)$ are calculated individually. In this way different time windows can be applied for each frequency. Time windows of $10/f$ are used.

2.1 Wavefield

The ambient vibration wavefield in urban areas is dominated by surface waves, with the relative content of Love and of Rayleigh waves unknown. The sources of the wavefield depend on the local conditions, but for urban areas they are generally assumed to be artificial and located at the surface. In this work we only analyse the vertical component, so we should only see the effect of Rayleigh waves. The fundamental mode usually dominates in urban areas, but in some cases higher modes can play an important role too.

In recent years the H/V polarization method (Nakamura 1989) has become quite popular in local site evaluation. Many authors (e.g. Yamanka *et al.* 1993; Lachet & Bard 1994; Fäh *et al.* 2001, 2003) have found the peak in the H/V polarization of ambient vibrations to be associated with the fundamental-mode Rayleigh wave. We use this method to verify the assumption that a significant amount of the fundamental-mode Rayleigh wave is present in the measured wavefield.

For the frequency range of 1–15 Hz most authors found the fundamental mode to be dominant when surficial sources were relevant, as is the case for the locations of interest near cities (Asten & Henstridge 1984; Yamanka *et al.* 1993, 1994; Lachet & Bard 1994;

Tokimatsu *et al.* 1992). A natural lower frequency limit is imposed on the method (using the vertical component only) by the polarization of the wavefield on the horizontal component at the fundamental frequency, where the vertical component contains no energy from the fundamental-mode Rayleigh wave. Fäh *et al.* (2001) suggest that in the range below the fundamental frequency of resonance the energy in the ambient vibrations can be distributed in other modes than the fundamental, so we cannot expect to determine dispersion below the fundamental frequency of resonance.

The HRBF estimator is applicable if the wavefield can be reasonably approximated as superposition of plane waves for the frequencies and phase velocities of interest. This implies that the resolvable signals have sources at distances an order of magnitude larger than the array aperture and that the local structure can be approximated with horizontal homogeneous layers. The useful signals for this method are dispersed and coherent over the array area, while signals which are non-coherent and not dispersed act as noise in the determination of surface wave dispersion.

Any coherent signal can be resolved by the estimator. For our application this implies that a significant content of body waves—which are coherent on the array—can increase the coherency at frequencies and wavenumbers not corresponding to the surface waves and thereby deteriorate the determination of surface wave dispersion.

2.2 Array configuration

The HRBF does not depend on a specific array configuration, but the wavenumber resolution properties of the array can be optimized through the configuration. Horike (1985) used L-shaped and cross-shaped arrays with a regular array spacing; irregularly spaced crosses were used by Asten & Henstridge (1984); Matsushima & Okada (1990); Milana *et al.* (1996) and many configurations consist of a series of symmetrically configured concentric triangles (Satoh *et al.* 2001a,b; Kawase *et al.* 1998). The number of stations used varies from four to 10 or more.

The theoretical properties of array configurations in seismology have been extensively studied for nuclear test ban treaty control as well as in practical applications (Carpenter 1965; Haubrich 1968). Barber (1959) and Haubrich (1968) showed ways in which the beam pattern can be understood and optimized for a given number of sensors. In general the array properties can be summarized by the following points:

(1) The higher the regularity the sharper the resolution of the array. Regularity means that distances between sensors are integer multiples of the smallest distance.

(2) The smallest detectable wavenumber is determined by the aperture of the array, with an improvement through the HRBF depending on the signal. The improvement of the resolution compared with regular beamforming is a factor of two to six, as reported by Asten & Henstridge (1984) and Horike (1985).

(3) The wavenumber aliasing in the f–$\mathbf{k}$ spectrum is determined through the smallest spacing between two sensors. If the spacing between sensors is not based on multiples of the shortest distance, the aliasing peak is lower in amplitude than the original peak.

There is no single optimal configuration for array measurements, but each configuration has some small advantages and disadvantages over others. The rule of thumb for choosing a configuration is to decide first on an aperture, depending on the largest phase velocities which have to be resolved, then the available sensors have to
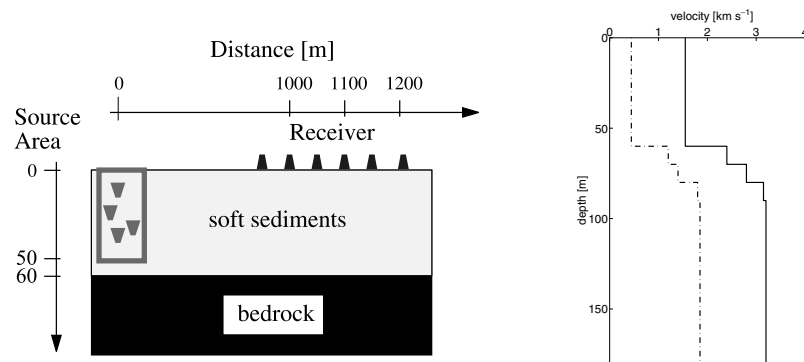
Figure 1. Model for the generation of synthetic ambient vibrations and the velocity structure modelled. The structure is 1-D and consists of 60 m of soft sediments overlaying bedrock. The density of the sediments is 1800 kg m^{-3} and that of the bedrock 2400 kg m^{-3}. Q_S is kept constant at 100, while Q_P changes from 200 in the sediments to 250 in the bedrock.

be configured in a balance of regularity (better resolution) and the creation of a wide spectrum of vector distances between the sensors (large coarray) for better aliasing properties.

3 SYNTHETIC TESTS

To validate our application of the HRBF technique and to illustrate some aspects of the data analysis we perform a test with synthetic data. The test targets the resolving strength of the algorithm in a complex wavefield composed of multiple wave types and sources, but with the basic assumptions for the applicability of the method intact. We generate realistic synthetic ambient vibrations using a 2-D finite-difference code (Fäh 1992). The algorithm is of second-order accuracy and is numerically stable for materials with normal as well as high Poisson's ratio. The simulated structure and sensor set-up is described in Fig. 1. The structure resembles to some extent the structure found at the first test site described later, but we do not draw conclusions about the measurement from the simulation.

The sources and wavefield composition of ambient vibrations are generally assumed to be surficial. Therefore we generate the synthetic wavefield with explosion-type point sources located randomly in a zone close to the left boundary of the finite-difference grid. Sources at a random depth of at most 50 m are allowed, to include possible conversions of wave types at lateral inhomogeneities and at layer interfaces. The configuration of the sensors is a regularly spaced line array with six sensors and a sensor spacing of 50 m, the first receiver being 950 m from the sources. For each receiver 240 s of signal are generated. Since a 2-D numerical scheme is used, the assumption of plane waves propagating through the array is inherently correct, independent of the source–receiver distance. The signals and their spectra are shown in Fig. 2.

The fundamental frequency of resonance of the simulated structure is at 1.85 Hz. Due to the nature of the sources, their location at the surface and the size of the grid used, only a small amount of energy is introduced below the fundamental frequency, as can be seen in the spectra.

Incoherent random signals with an equivalent spectrum to the synthetic data were superposed on the synthetics so as to test the robustness of the estimator against the contamination of the wavefield through various mechanisms. Strong body wave signals could be present covering the surface waves, or the numerous partial signals of the ambient vibration wavefield together with the segmentation of
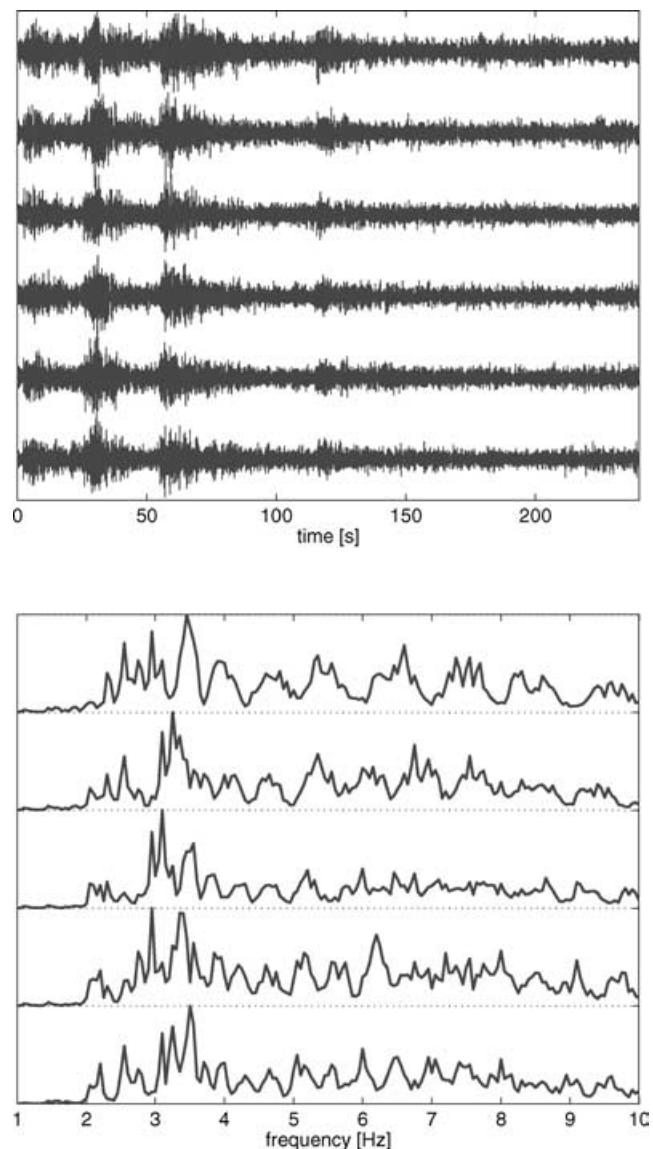

Figure 2. Synthetic data used to test the HRBF. The upper part shows the signals and the lower part the spectra. Hardly any energy is present below 1.85 Hz, as would be expected for the excitation of fundamental-mode Rayleigh waves with surficial sources.
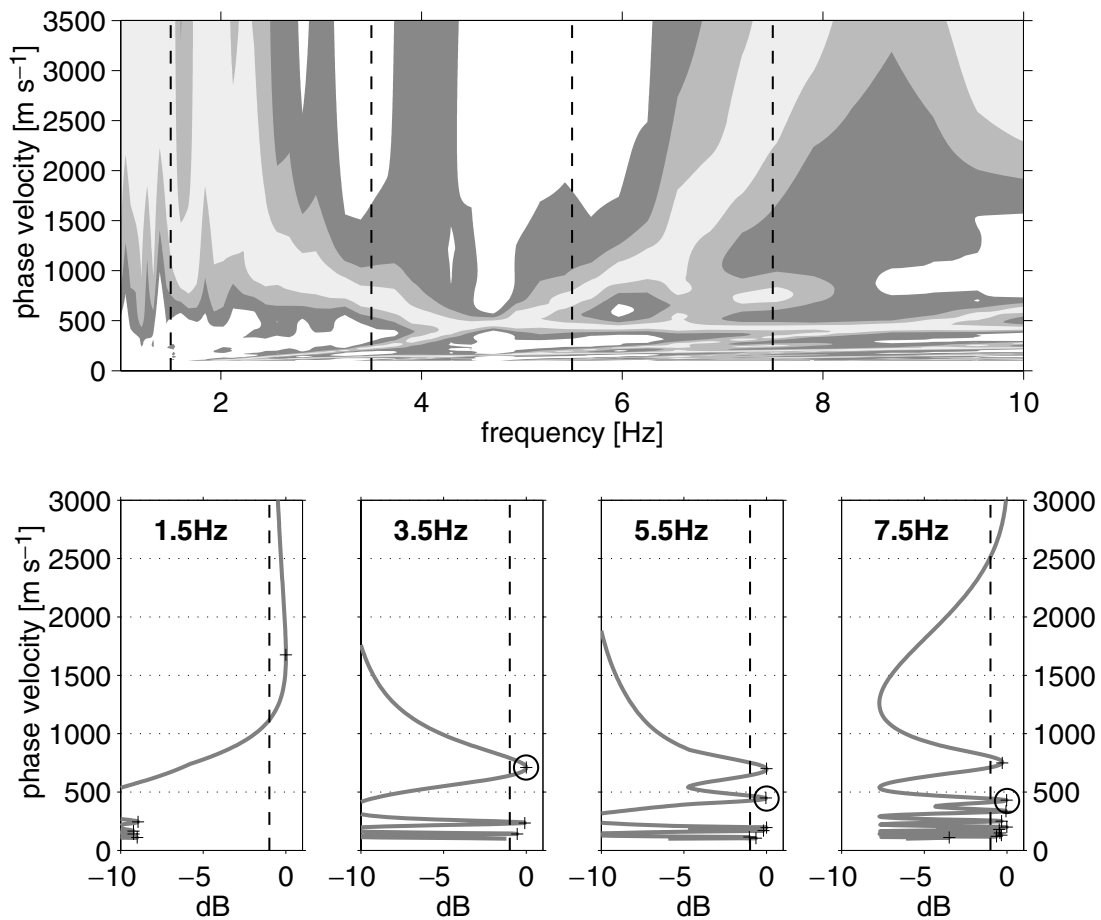
Figure 3. Extraction of the dispersion curve. The upper part of the figure shows the frequency–phase velocity (*f–c*) diagram. For this the maximum over the azimuth is taken from the *f*–**k** spectrum, the values for each frequency are normalized to the maximum and the resulting spectrum of the azimuthal maxima is shown against frequency and phase velocity. Contours of −5, −3 and −1 dB are shown. Four dashed lines indicate the frequency sections shown in the lower part of the figure. The dispersion curve is extracted by manual selection of a local maximum so as to avoid the aliases, as explained in the text.

the signals for the coherency estimation might lower the coherency of the signals of interest considerably. This superposition of white noise should not be confused with the numerical stabilization of the HRBF method in the case of insufficient recording length of the available data (Capon 1969), which can be done through the addition of a small amount of noise. In our case the recording length is long enough and the amount of noise added is large (equivalent to the actual signal), showing the performance of the method under adverse conditions.

The *f*–**k** spectrum was calculated for wavenumber ranges corresponding to the velocity range (200–3500 m s⁻¹) at each frequency and for both directions. The size of the time window used in the analysis was 10 times the period of the respective frequencies considered; the whole 240 s were analysed for one *f*–**k** estimation. The resulting *f*–**k** spectrum is normalized at each frequency level to the maximum spectral value at this frequency. For the visualization of the spectrum in the upper part of Fig. 3 the **k** scale is converted to the corresponding phase velocities (*f*–*c* diagram). In grey scale the contours of the −1, −3 and −5 dB levels are shown, a decibel being defined here as $20 \times \log 10$. The lower part of the same figure shows the normalized azimuthal maxima (or sections of the *f*–*c* diagram) at four frequency levels. The location of the sections is indicated in the *f*–*c* diagram with dashed lines. The dispersion curve is determined by visual inspection of these levels under the following rules:

(1) Only local maxima from the curve are selected.

(2) The resulting dispersion curve is continuous and follows a single ridge of locally maximal amplitude in the *f*–*c* diagram.

(3) No value is determined if the amplitude of the curve at the high-velocity end of the peak is more than −1 dB (see Fig. 3, 1.5 Hz).

The manual interpretation is necessary to avoid aliasing, which is made purposely strong in the chosen example configuration of a short and regular line array, but is also important in the later measurements. The second rule is not generally fully applicable and can lead to erroneous interpretation if an inversion for *P*-wave velocities and detailed resolution are also looked for in special sediment structures (Forbiger 2001). But in the context of seismic hazard studies with a focus on *S*-wave velocities on a coarse resolution scale it is a fair assumption.

Fig. 4(a) then shows the *f*–*c* diagram of the synthetic wavefield together with the theoretical fundamental-mode and first higher-mode Rayleigh wave dispersion as thick black lines and the dispersion curve determined from the HRBF estimation as a series of circles. Below (Fig. 4b) the relative difference between the phase velocities determined by the estimation and the theoretical value is indicated. The error remains well below 10 per cent of the phase velocity in most cases. Despite the aliasing at higher frequencies, the dispersion curve can be quite well determined through manual
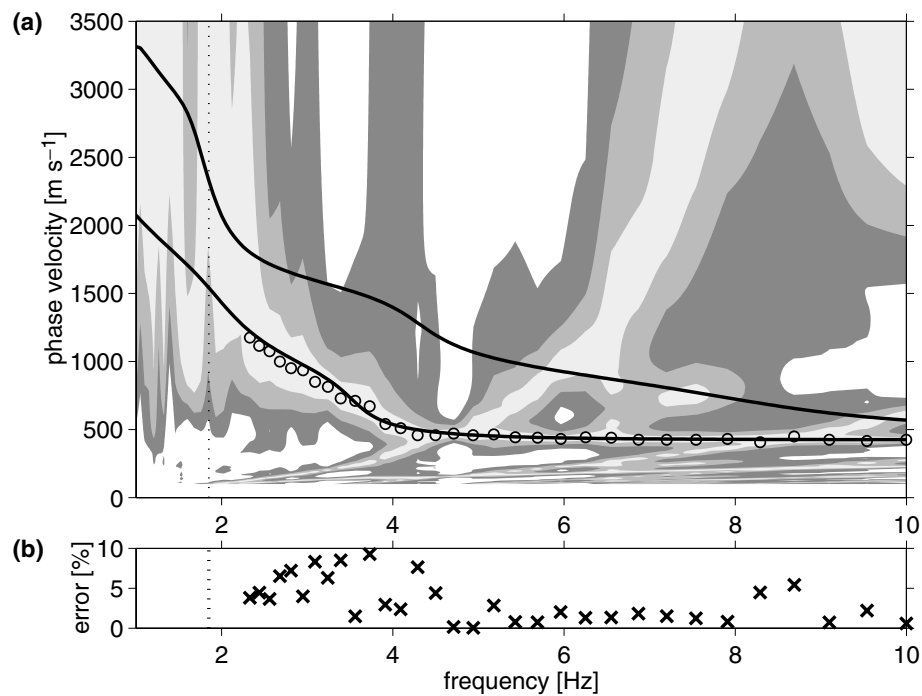
Figure 4. Comparison of the extracted dispersion (circles) with the theoretical values (continuous lines). The first higher-mode Rayleigh wave is also shown and can be identified in the interval 6–8 Hz. Below 2 Hz no phase velocity can be determined, as the Rayleigh wave polarizes on the horizontal at the fundamental frequency of 1.85 Hz and therefore no energy from the fundamental-mode Rayleigh wave is present on the vertical component. The errors in the determination are given as a percentage of the theoretical phase velocities.

interpretation. A first higher mode is partially visible in the frequency range 6–8 Hz. In the real measurements a higher mode would probably be more difficult to identify, so we do not look for such features in the later measurements.

The fundamental frequency of resonance of the structure is at 1.85 Hz, indicated with a vertical dotted line in Fig. 4. The dispersion curve can be determined down to 2.2 Hz; at lower frequencies no phase velocity can be determined. This is consistent with the absence of energy in the spectra of the signals below the fundamental frequency and with the domination of the fundamental Rayleigh wave, which polarizes on the horizontal component at the fundamental frequency.

In a further test the amount of random signal added to the synthetics was varied between zero and 100 per cent, to quantify how much coherent signal has to be present to allow for the determination of the dispersion curve. The results for four frequencies are shown in Fig. 5. For each frequency the normalized azimuthal maxima curves, as shown in the lower part of Fig. 3, are combined from all noise levels into a surface. The figures show estimated energy content against phase velocity and the percentage of uncorrelated noise. A black vertical line indicates the theoretical phase velocity. Clearly, the quality of the identification of the phase velocity remains constant for a content of up to 60 per cent uncorrelated signals and even more for the higher frequencies.

4 HARDWALD TEST SITE

4.1 Site and measurements

To test the HRBF in real conditions a measurement was made at the Hardwald site just outside the city of Basel, Switzerland (Fig. 6). The site is a light forest of 3 km² in a drinking water protection area

near the River Rhine. No roads or industry are within a distance comparable to the array aperture, so the approximation of the wavefield with plane waves is as good as it can be within a populated area. An industrial area is located a few kilometres to the northeast of the location, a major motorway passes at a distance of over a kilometre to the southwest and a few kilometres to the northwest lies the city of Basel, so enough surficial sources are present to generate surface waves. The geology down to the bedrock is well known from many boreholes drilled for ground water control.

The site is characterized by 35 to 40 m of Quaternary gravels above the bedrock consisting mostly of Triassic chalks with some small graben structures of Keuper and Lias. The approximation of horizontal layering applies well to the site and the topography is flat with small irregularities in the order of 1 m. The average shear wave velocities are known from literature values as 300–500 m s⁻¹ in the gravels and 1000–2200 m s⁻¹ in the bedrock, giving a strong S-wave velocity contrast (Fäh *et al.* 1997). This is confirmed by the H/V polarization analysis of the array sensor data, shown in Fig. 7. The curves are very uniform below 2.5 Hz, while they vary slightly in the higher frequencies. The clear, high-amplitude peaks indicate a strong velocity contrast at the bedrock. As the H/V ratio peak is associated with the fundamental-mode Rayleigh wave, the H/V curve also indicates that a significant contribution to the wavefield is from the fundamental-mode Rayleigh wave (Yamanka *et al.* 1994; Fäh *et al.* 2001, 2003). The variations towards higher frequencies suggest slight lateral inhomogeneities in the surface layer, as would be expected in alluvial gravels.

Thirteen sensors with an eigenperiod of 1 s in a configuration of four circles of three stations plus one central station were deployed. The radii of the circles are approximately 40, 50, 80 and 100 m, resulting in an aperture of 180 m. The configuration is given in Fig. 8. The precision of the timing synchronization of the instruments was
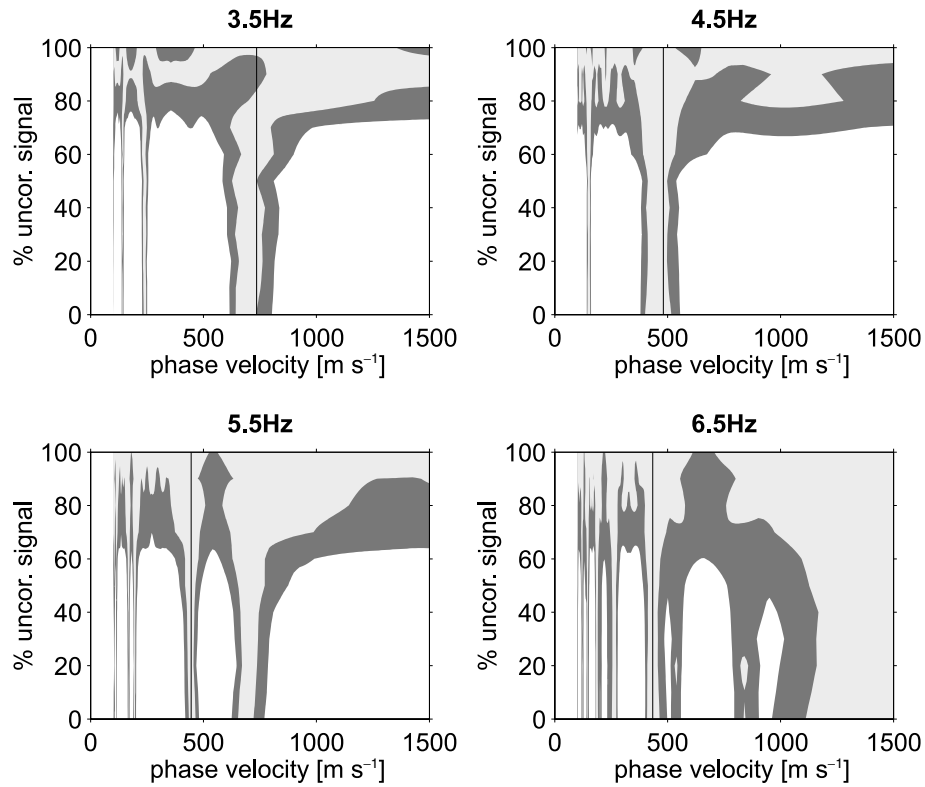
Figure 5. Spectral amplitudes at four different frequencies from the analysis of synthetic signals with a varying portion of uncorrelated signal. The vertical black lines indicate the theoretical phase velocity. Contours of −5, −3 and −1 dB are shown in grey scale.
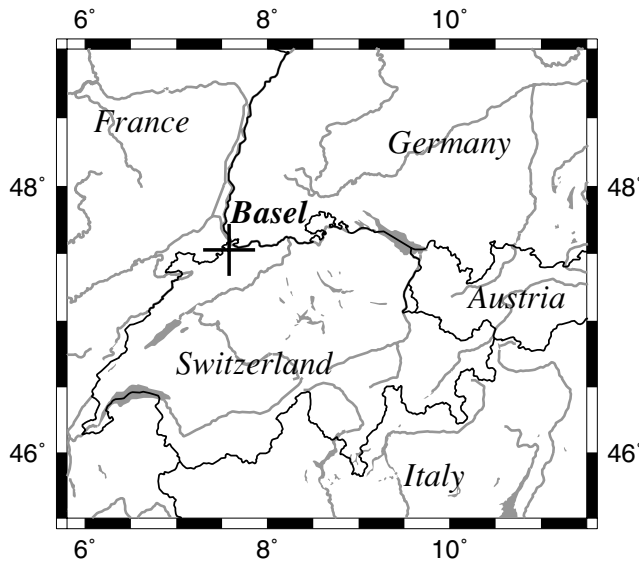

Figure 6. Location of the test site within Europe. The site is just outside the city limits of Basel.

tested to be ±1 ms. A data set was recorded during daytime with a 2 ms sampling interval for 6 min. In the HRBF analysis the range 1–10 Hz is analysed at 50 logarithmically distributed frequencies. The wavenumber sampling is done with a grid in polar coordinates with a directional resolution of 2.5° and a wavenumber sampling corresponding to a phase velocity range of 100–3500 m s^{-1} in varying steps of 5, 10 and 25 m s^{-1}, so as to avoid mismatch in the f–$\mathbf{k}$

estimation due to grid steps which are too large. The time windows for the Fourier transform correspond to 10 times the period, as indicated previously. The analysis is done over one whole recording of 6 min as the estimate of the coherency becomes more reliable for a longer duration, as described in Capon (1969).

The wavefield for the whole recording time is composed of signals coming from all directions. This is shown at two frequency levels in Fig. 9. North is at the top of the figure. In the lower frequencies the signals from the industry and the city are somewhat stronger then those from the motorway; in the higher frequencies the signals from the city and the motorway dominate. The ridge in the f–$\mathbf{k}$ spectrum is very distinct and the phase velocity is identified at the wavenumber indicated with the circles. The deviations from the circular form at the higher frequency illustrate how the small-scale heterogeneities of the structure become more relevant for shorter wavelengths. The validity of the approximation by a 1-D structure is confirmed by the circular form of the high-energy ridge.

The maximum over the azimuth is taken from the f–$\mathbf{k}$ spectrum; at each frequency the spectrum is normalized to its maximum and the wavenumber values are converted to phase velocity, so as to create the f–c diagram shown in Fig. 10. The contours for −5, −3 and −1 dB are shown. The dispersion curve was extracted as demonstrated for the synthetic data and is given as small circles. The identification is quite clear as aliasing peaks are reduced through the irregularity in the configuration, but misinterpretations are still a danger at higher frequencies. The vertical dotted line indicates the fundamental frequency of the site as determined in the H/V ratios. Slightly above this frequency the phase velocity can no longer be determined, consistent with the polarization on the horizontal of the Rayleigh wave.
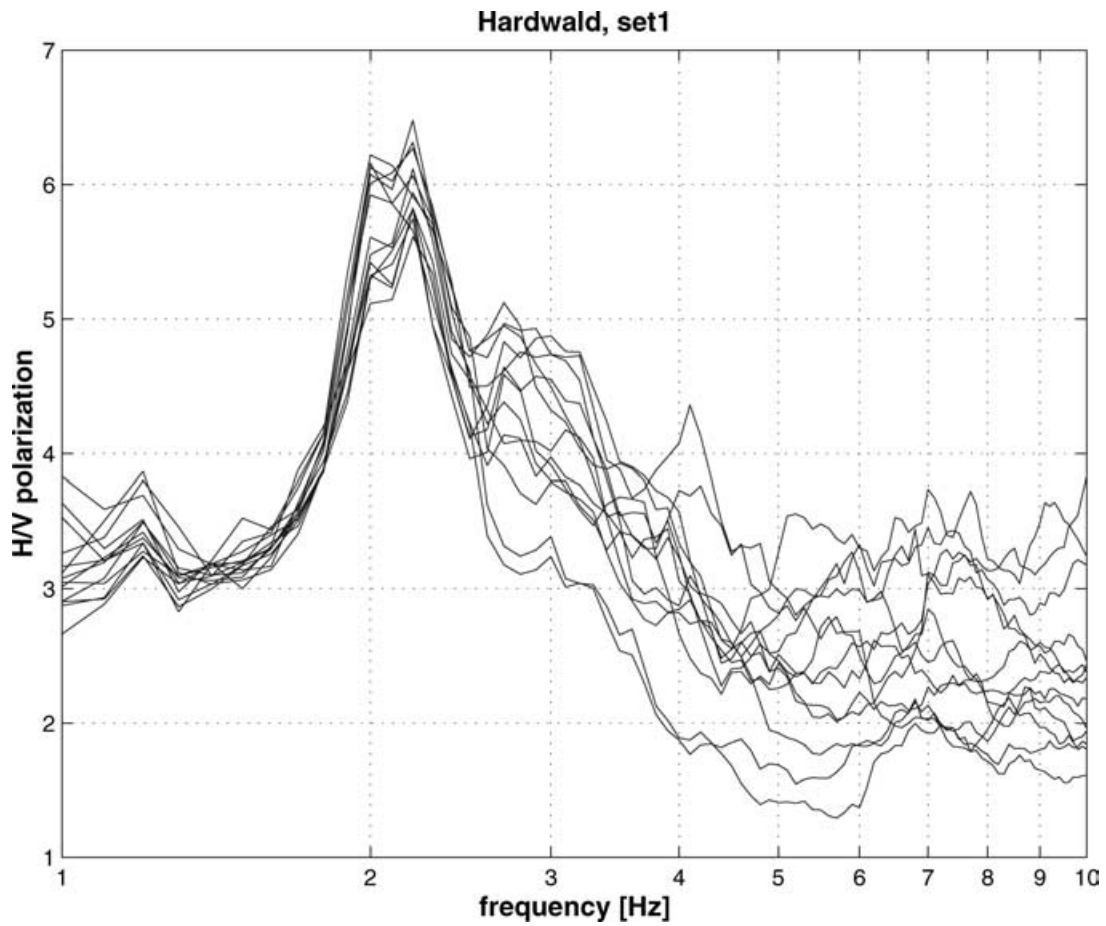
Figure 7. Overlay of the H/V polarization analysis of the data at each of the 13 sensors in the array. The fundamental frequency is at 2.2 Hz.
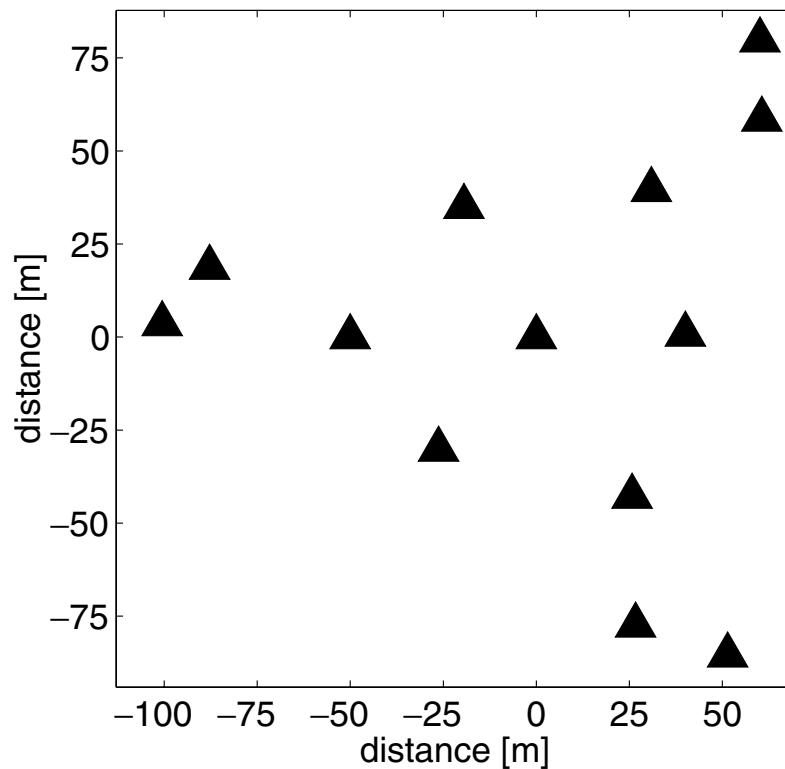

Figure 8. Configuration of the array at the first test site. Four circles of three sensors plus a central station are deployed. The radii of the circles were roughly 40, 50, 80 and 100 m.
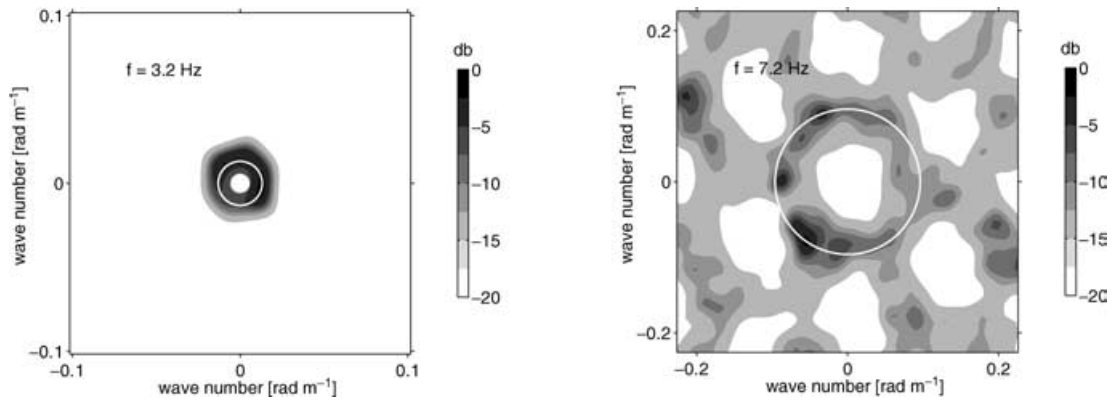
Figure 9. Two sections of the f–**k** spectrum at frequencies of 3.2 and 7.2 Hz. The ambient vibration wavefield is composed of signals from almost all directions at the same time. North is at the top of the figure and west and east to the left and right respectively. The circle indicates the identified phase velocity.
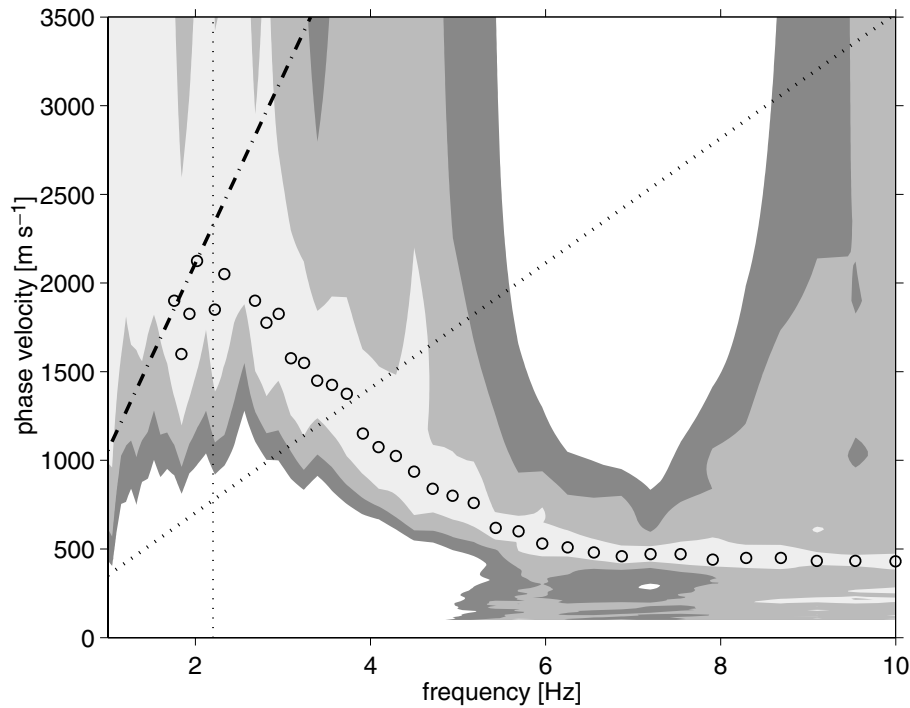

Figure 10. f–c diagram for the Hardwald test site with contours of -5, -3 and -1 dB. The circles are the local maxima identified for the dispersion curve. A vertical dotted line indicates the fundamental frequency of resonance of the structure, the inclined dotted line shows the theoretical limit of the beamforming resolution and the dashed-dotted line indicates the rule of thumb of an improvement by a factor of three for the HRBF. Here the polarization of the Rayleigh wave on the horizontal limits the determination of the dispersion curve to the fundamental frequency of resonance.

The diagonal dotted line indicates the theoretical beamforming resolution limit defined through the aperture, while the dashed-dotted line corresponds to a resolution which is three times higher. The last identified phase velocities around and below the fundamental frequency follow the dashed-dotted line. This indicates an alias of the wavenumber zero resulting when the resolution limit is reached. The rule of thumb of a factor of three improvement over the theoretical resolution limit for beamforming given by Horike (1985) is supported by this data, but the coincidence with the absence of energy on the vertical component at the fundamental frequency interferes with the resolution limit.

4.2 Inversion

Our application aims at the derivation of *S*-wave velocities as they are needed for the assessment of local site effects in seismic hazard

studies. A number of inversion algorithms and strategies are available and we choose one arbitrarily to illustrate the possibilities of the f–**k** spectrum with the inversion results. At the moment we only use the dispersion of the fundamental-mode Rayleigh wave from the vertical component for the inversion. By looking at the second mode and the horizontal component, the method can be improved further.

The inversion scheme we use is a genetic algorithm procedure. The layer thickness and *S*-wave velocity of seven layers for the unconsolidated sediments and for two bedrock layers are selected as free parameters. The maximum depth of the sediments with *S* velocities below 1400 m s^{-1} is limited to 144 m. Due to the non-uniqueness of the solution, several runs are performed with different ranges for the layer parameters and different weights to the segments of the dispersion curve during the inversion. The dispersion curve
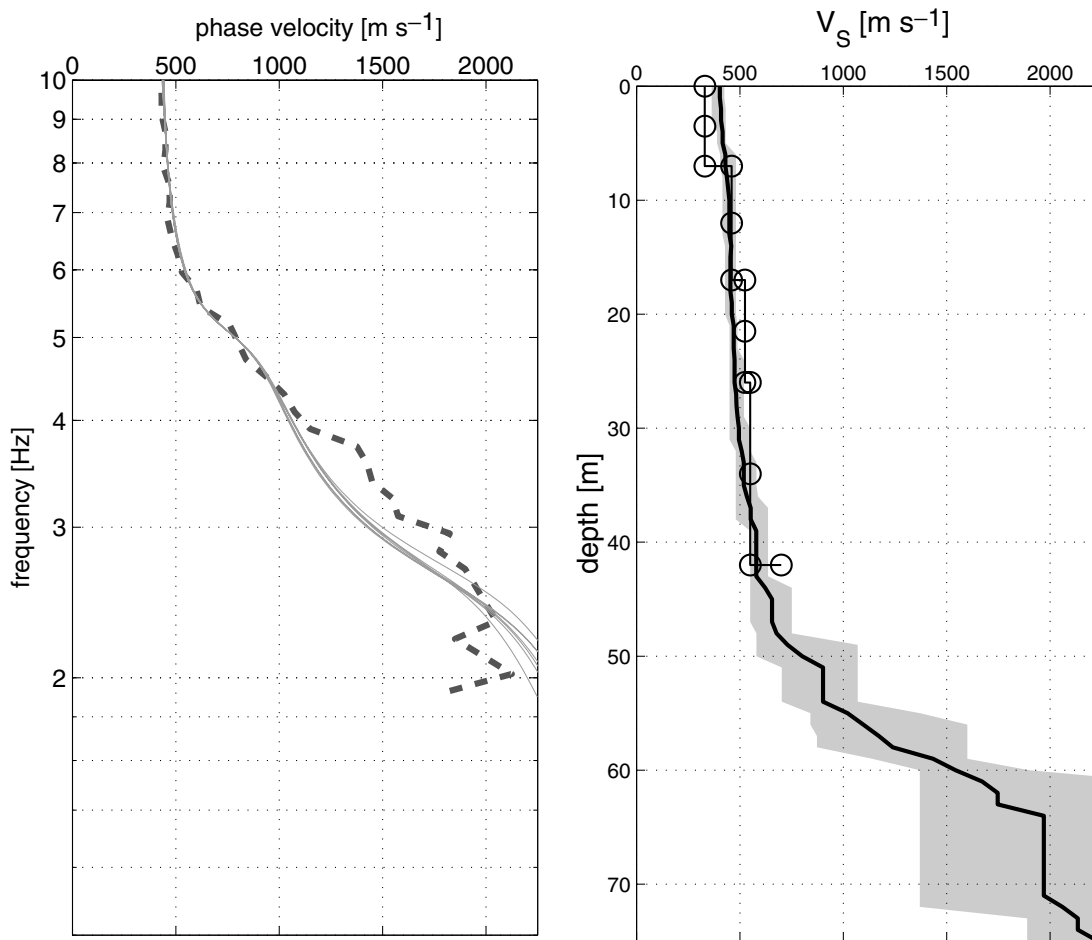
Figure 11. Results from the inversion of the data from the test site at Hardwald. On the left the thick dashed line shows the dispersion result from the test measurement. Superposed as thin continuous lines are the dispersion curves from the inversion results. On the right-hand side the corresponding average velocity profile of the inversion results is shown with the range of models indicated as a grey shaded area. An average reference *S*-wave velocity structure from a reflection survey at the site is given as circles joined with a thin line.

was calculated with modal summation (Panza 1985) for all models in each iteration and the difference from the measured dispersion used as the fitness function. The models were improved iteratively, resulting in several plausible models. The inversion result is by nature non-unique and with the scheme used we do not have much control on the absolute error. The great advantage of the approach used is the simplicity and speed with which a reasonable result is reached.

The dispersion of the best-fitting models resulting from seven inversion runs is plotted in Fig. 11 on the left as thin lines superposed on the dispersion extracted from the f–**k** spectrum (dashed line). The corresponding average shear wave velocity structure of the inversion results is given as a black line on the right, with the range from the inversions as a grey shaded area. The first 35–45 m with shear wave velocities between 400 and 500 m s^{-1} are typical for the Quaternary gravels in this area. The depth range is slightly higher than expected, but is in general agreement with the information from surrounding boreholes at distances of about 100–200 m from the array test site, suggesting about 35–40 m of gravels. We interpret the following 25 m with a strong gradient as the eroded surface of the bedrock. The shear wave velocity of the bedrock is consistently very high, in good agreement with the literature values in the range of 1000–2200 m s^{-1}. The high contrast is also in excellent agreement with the large H/V polarization peaks in Fig. 7.

At the site of the array measurement an experimental shear wave seismic reflection line has also been set up (F. Nitsche, Institute for Geophysics, ETH Zürich, Switzerland, unpublished results). The right-hand side of Fig. 11 shows the resulting average *S*-wave velocity structure from this experiment as a thin line connecting circles. They represent evaluations of the *S*-wave velocity profile from four points across the array. The values correspond very well with the inversion results from the dispersion curve measured with the array. They also illustrate an important advantage of the method compared with conventional borehole or reflection seismic *S*-wave techniques: conservatively we get results from inversion to a depth of about half the aperture of the array using a very inexpensive method.

5 THE INDUSTRIAL TEST SITE

Another test was performed at a second site. This site lies within an industrial complex, where V_S data from cross-hole measurements within the Quaternary sediments were available. The measurement was done on a small patch of grass of very limited size, therefore the size of the array was reduced to seven sensors and a diameter of less than 40 m. The configuration is shown in Fig. 12. Information from boreholes indicates 20–30 m of Quaternary gravels above calcareous Tertiary bedrock. The buildings of the complex start at a distance
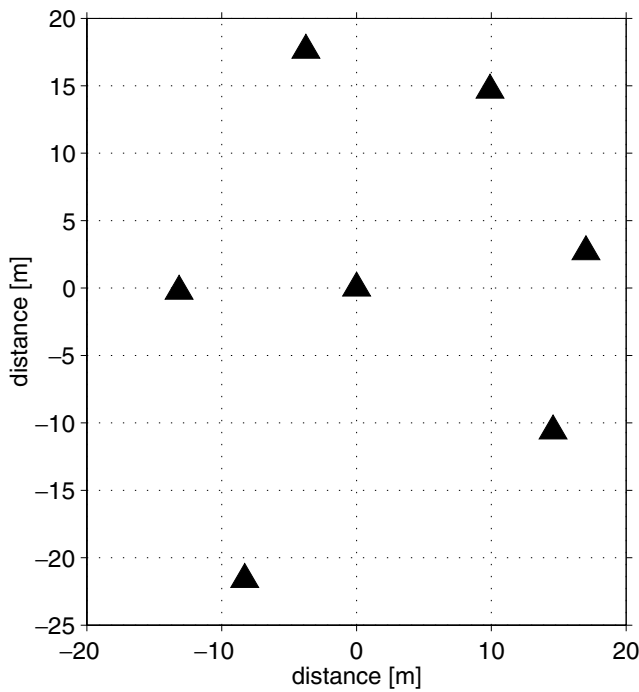
Figure 12. Configuration of the array at the industrial test site. Due to the limited space only seven sensors were deployed.

of the order of one array aperture away, such that the plane wave assumption is at a limit for these sources.

Again, we want to find out if the H/V ratio from all sensors (Fig. 13) indicates that the ambient vibrations contain a significant part of the fundamental-mode Rayleigh waves (Yamanka *et al.* 1994; Fäh *et al.* 2001, 2003). The uniformity of the H/V curves supports the 1-D approximation for the site. As the fundamental frequency is about 4.2 Hz we apply the HRBF in the range 3–15 Hz; the f–c diagram is shown in Fig. 14.

With the rules for the extraction of the dispersion curve laid down for the synthetic example, phase velocities can be extracted up to 5 Hz, close to the fundamental frequency. The theoretical resolution limit from beamforming is given as a dotted line in Fig. 14, while the rule of thumb of three times better resolution with the HRBF results is shown by the dashed-dotted line. This resolution limit is met here.

The result from the inversion is shown in Fig. 15. On the left are the extracted dispersion curve as a dashed line and the inverted models as thin lines; on the right the average resulting V_S structure is shown with the range of variation in the models shown in grey. After the measurement we had access to the unpublished results of a cross-hole experiment that was performed about 30 yr previously, before the construction of the industrial complex. The borehole sites were located some tens of metres away from the array centre. Two experiments were performed at that time, with three boreholes. The distance between two boreholes was between 6.2 and 7.9 m. The
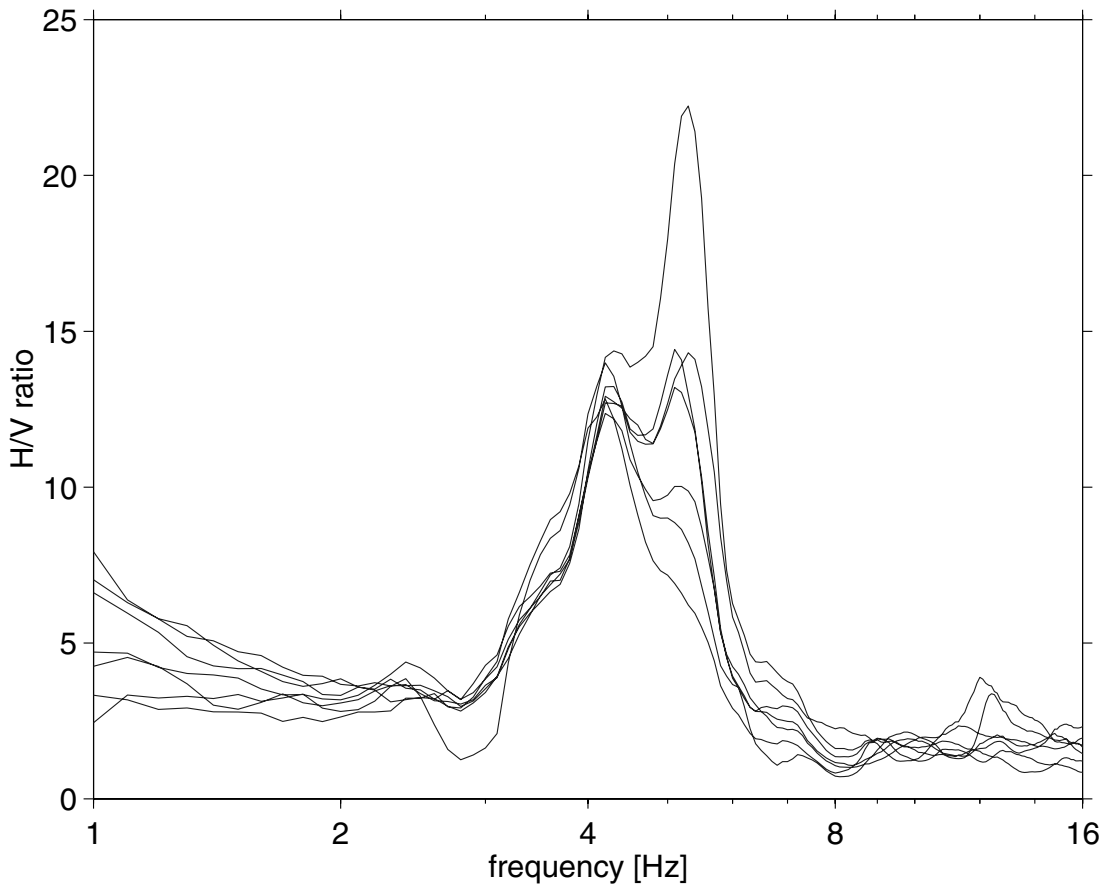
Figure 13. Overlay of the H/V polarization analysis of the data at each of the seven sensors in the array. The fundamental frequency is at 4.2 Hz.
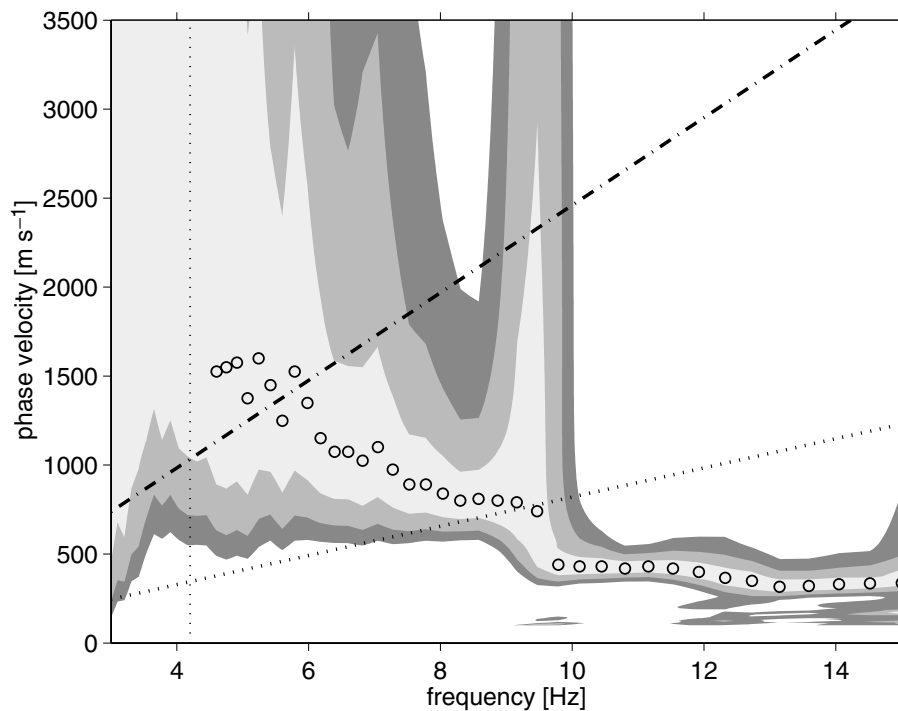
Figure 14. *f*–*c* diagram for the industrial test site with contours of −5, −3 and −1 dB. The circles are the local maxima identified for the dispersion curve. A vertical dotted line indicates the fundamental frequency of resonance of the structure, the inclined dotted line shows the theoretical limit of the beamforming resolution and the dashed-dotted line indicates the rule of thumb of an improvement by a factor three for the HRBF. In this case the dashed-dotted line marks the limit where the dispersion curve can be determined.

resulting *S*-wave velocities are shown as circles, with an estimated error of up to 20 per cent in the cross-hole measurements. The *S*-wave velocities and their variability is exactly in the range of the results obtained from the array inversion.

6 CONCLUSIONS

The applicability of the use of high-resolution beamforming to derive phase velocities from ambient vibrations was tested. Tests with synthetic ambient vibrations confirm the capability of the method to extract the correct phase velocities of the excited Rayleigh mode. The observed errors were less than 10 per cent and the dispersion can be determined even if the wavefield consists of up to 60 per cent of uncorrelated signals. Therefore no signal selection has to be done on a recording if a significant contribution of fundamental-mode Rayleigh wave energy is present in the ambient vibrations, as is usually the case for urban areas. But the sites have to be carefully selected to meet the requirement of large source distances compared with the array diameter.

A measurement at a site close to the city of Basel in Switzerland illustrates the applicability of the method. The dispersion curve of the fundamental-mode Rayleigh wave was determined from the fundamental frequency of resonance upwards, consistently in the synthetics as well as in the measurements. The rule of thumb of a factor of three improvement in the resolution of the HRBF compared with the theoretical resolution of the beam pattern could be confirmed. The inverted *S*-wave velocity structure corresponds well to data from an *S*-wave reflection survey and the geological information for the site. At a second test site with a much smaller array the test could be repeated, confirming the results from the first test.

The array technique is a very cost-effective and time-efficient tool for measuring *S*-wave velocities, as only half a day of field work and 2 to 3 days of data processing are needed for a measurement. The only *a priori* information needed for its application is whether the site can be approximated as a 1-D structure. For the study of local earthquake hazard and in deterministic modelling of earthquake scenarios the lack of *S*-wave velocity information is often a source of large uncertainties. This array technique and other methods based on ambient vibrations are a step towards making seismic zonation feasible through numerical modelling of site effects.

REFERENCES

Asten, M.W. & Henstridge, J.D., 1984. Array estimators and the use of microseisms for reconnaissance of sedimentary basins, *Geophysics,* **49**(11), 1828–1837.
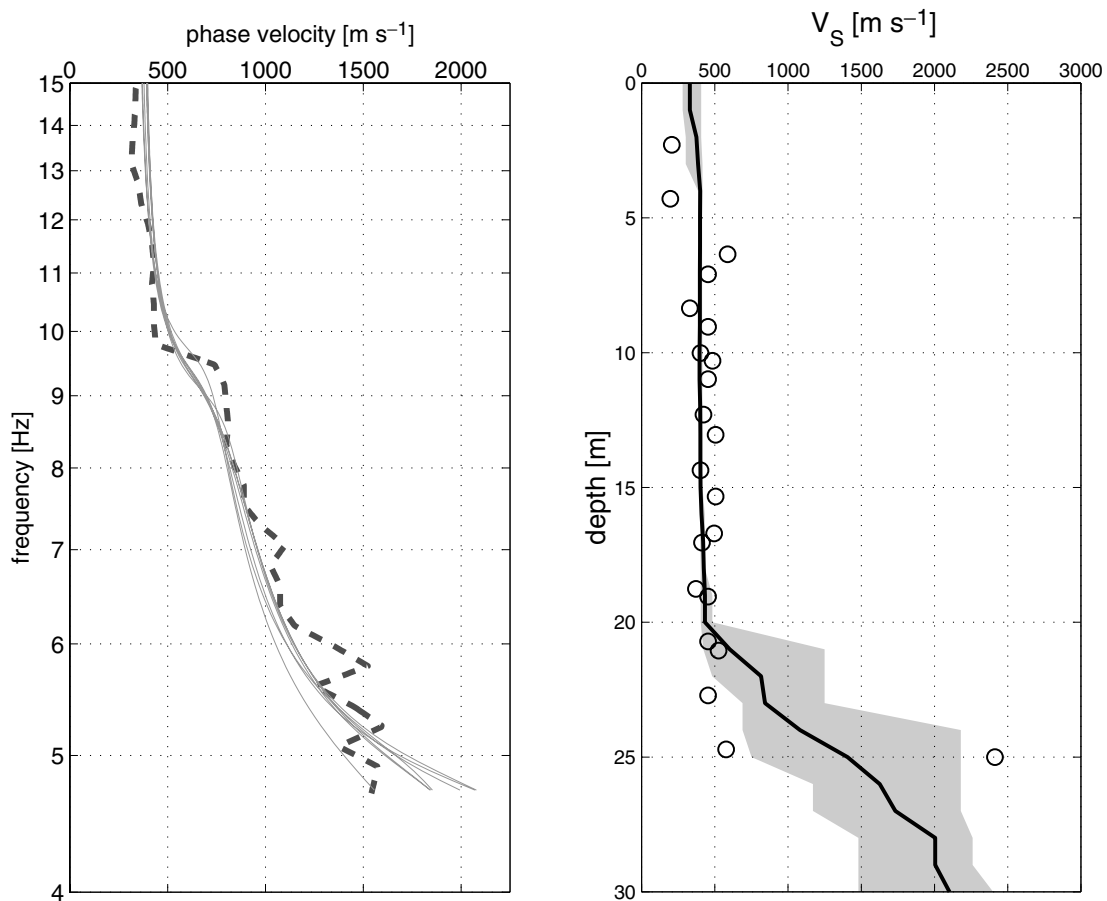
Figure 15. Results from the inversion of the data from the industrial test site. On the left the thick dashed line shows the dispersion result from the measurement. Superposed as thin continuous lines are the dispersion curves from the inversion results. On the right-hand side the corresponding average velocity profile of the inversion results is shown with the range of models indicated as grey shaded area. Circles indicate the *S*-wave measurement results from a previous cross-hole experiment.

Barber, N.S., 1959. Design of 'optimum' arrays for direction finding, *Electron. Radio Eng.,* **36,** 222–232.

Capon, J., 1969. High-resolution frequency-wavenumber spectrum analysis, *Proc. IEEE,* **57,** 1408–1418.

Carpenter, E.W., 1965. A historical review of seismometer array development, *Proc. IEEE,* **53,** 1816–1833.

Fäh, D., 1992. A hybrid technique for the estimation of strong ground motion in sedimentary basins, *PhD thesis,* No 9767, Swiss Federal Institute of Technology (ETH) Zürich.

Fäh, D. J., Rüttener, E., Noack, T. & Kruspan, P., 1997. Microzonation of the city of Basle, *J. Seism.,* **1,** 87–102.

Fäh, D., Kind, F. & Giardini, D., 2001. A theoretical investigation of average H/V ratios, *Geophys. J. Int.,* **145,** 535–549.

Fäh, D., Kind, F. & Giardini, D., 2003. Inversion of local S-wave velocity structures from average H/V ratios, and their use for the estimation of site-effects, *J. Seism.,* **7,** 449–467.

Forbiger, T., 2001. Inversion flachseismischer Wellenfeldspektren, *PhD thesis,* Institut für Geophysik, Universität Stuttgart.

Haubrich, R.A., 1968. Array design, *Bull. seism. Soc. Am.,* **58,** 977–991.

Horike, M., 1985. Inversion of phase velocity of long-period microtremors to the S-wave-velocity structure down to the basement in urbanized areas, *J. Phys. Earth,* **33,** 59–96.

Kawase, H., Satoh, T., Iwata, T. & Irikura, K., 1998. S-wave velocity structure in the San Fernando and Santa Monica areas, in *The Effects of Surface Geology on Seismic Motion,* pp. 733–740, eds Kudo, K., Okada, H. & Sasatani, T., Balkema, Rotterdam.

Lachet, C. & Bard, P.-Y., 1994. Numerical and theoretical investigations on the possibilities and limitations of Nakamura's technique, *J. Phys. Earth,* **42,** 377–397.

Lacoss, R., Kelly, E. & Toksöz, M., 1969. Estimation of seismic noise structure using arrays, *Geophysics,* **34,** 21–38.

Liu, H.-P., Boore, D., Joyner, W., Oppenheimer, D., Warrick, R., Zhang, W., Hamilton, J. & Brown, L., 2000. Comparison of phase velocities from array measurements of Rayleigh waves associated with microtremor and results calculated from borehole shear-wave velocity profiles, *Bull. seism. Soc. Am.,* **90,** 679–689.

Matsushima, T. & Okada, H., 1990. Determination of deep geological structures under urban areas using long-period microtremors, *Butusuri-Tansa,* **43,** 21–33.

Milana, G., Barba, S., Del Pezzo, E. & Zambonelli, E., 1996. Site response from ambient noise measurements: new perspectives from an array study in central Italy, *Bull. seism. Soc. Am.,* **86,** 320–328.

Nakamura, Y., 1989. A method for dynamic characteristics estimation of subsurface using microtremor on the ground surface, *Q. Rep. Railway Tech. Res. Inst., Tokyo,* **30,** 25–33.

Panza, G.F., 1985. Synthetic seismograms: the Rayleigh waves modal summation, *J. Geophys.,* **58,** 125–145.

Ramirez, J.E., 1940. An experimental investigation of the nature and origin of microseisms at St Louis, Missouri, *Bull. seism. Soc. Am.,* **30,** 139–178.

Satoh, T., Kawase, H. & Matsushima, S., 2001a. Estimation of S-wave velocity structures in and around the Sendai basin, Japan, using array records of microtremors, *Bull. seism. Soc. Am.,* **92,** 2, 206–218.

Satoh, T., Kawase, H. & Matsushima, S., 2001b. S-wave velocity structure of the Taichung basin, Taiwan, estimated from array and single-station records of microtremors, *Bull. seism. Soc. Am.,* **91,** 5, 1267–1282.

Tokimatsu, K., 1997. Geotechnical site characterization using surface waves, in *Earthquake Geotechnical Engineering,* pp. 1333–1368, ed. Ishihara, K., Balkema, Rotterdam.

Tokimatsu, K., Shinzawa, K. & Kuwayame, S., 1992. Use of short-period microtremors for V_s profiling, *J. Geotech. Eng.,* **118,** 1544–1558.

Toksöz, M., 1964. Microseisms and an attempted application to exploration, *Geophysics,* **24,** 154–177.

Yamanka, H., Dravinski, M. & Kagami, H., 1993. Continuous measurements of microtremors on sediments and basement in Los Angeles, California, *Bull. seism. Soc. Am.,* **83,** 1595–1609.

Yamanka, H., Takemura, M., Ishida, I. & Niwa, M., 1994. Characteristics of long-period microtremors and their applicability in exploration of deep sedimentary layers, *Bull. seism. Soc. Am.,* **84,** 1831–1841.